# High-throughput single cell manipulation and picoliter scale sampling of cell cultures

## (Report 2018.12.01.-2022.11.30.)

### High-throughput single cell isolation into standard multi-well plates

One of the aims of my research is to achieve high speed, high-throughput single cell isolation technique for RNA/DNA sequencing. Single cells are the basic units of life. Studying them helps to understand predisposition to diseases, to choose the appropriate therapy, allows understanding heterogeneity between cells and structure and operations of tissues. A deeper understanding of a developing embryo or tumor requires molecular information on the constituting individual cells. It is important to enable high-throughput studies using multi-well plates, which will be useful in the medical diagnostics and testing of drugs, as well.

The CellSorter single cell isolation system[1,2] can isolate adherent individual cells into PCR tubes or onto a glass coverslip with a sorting speed of 3-4 cells/min, while cell sorting into multi-well plates is slower: 2 cells/min. Thus the isolation of 100 cells would take ~ 50 min, during which time the cells can be damaged without incubation. The goal was to apply the CellSorter micropipette to isolate ≥100 single cells based on their microscopic image into a standard multi-well plate within 15 min. Currently available single cell sorting robots cannot complete this task.

The selected individual cells were picked up from a Petri dish one-by-one based on their previously detected microscopic image with an inner diameter (I.D.) of 70 μm glass micropipette. During the picking process, single cells in the aqueous medium were separated from each other with a spacer oil (mineral oil) layer to avoid the mixing of the individual cells inside the micropipette (**Fig 1**).

The volume of the picked-up aqueous drop is a crucial parameter in the downstream investigation of cells, e.g., sequencing uses expensive reagents. In order to minimize the drop volume to reach the submicroliter regime, the same vacuum value (-9,000 Pa) was used as in our standard protocol[2]. However, due to the high viscosity of the oil, I encountered technical problems. The oil could be sucked into the micropipette very slowly. Increasing the vacuum, the spacer oil could be sucked up into the tip in less time, however, cells in the aqueous medium were picked up in a larger volume, and neighboring cells were also picked up by the pipette.

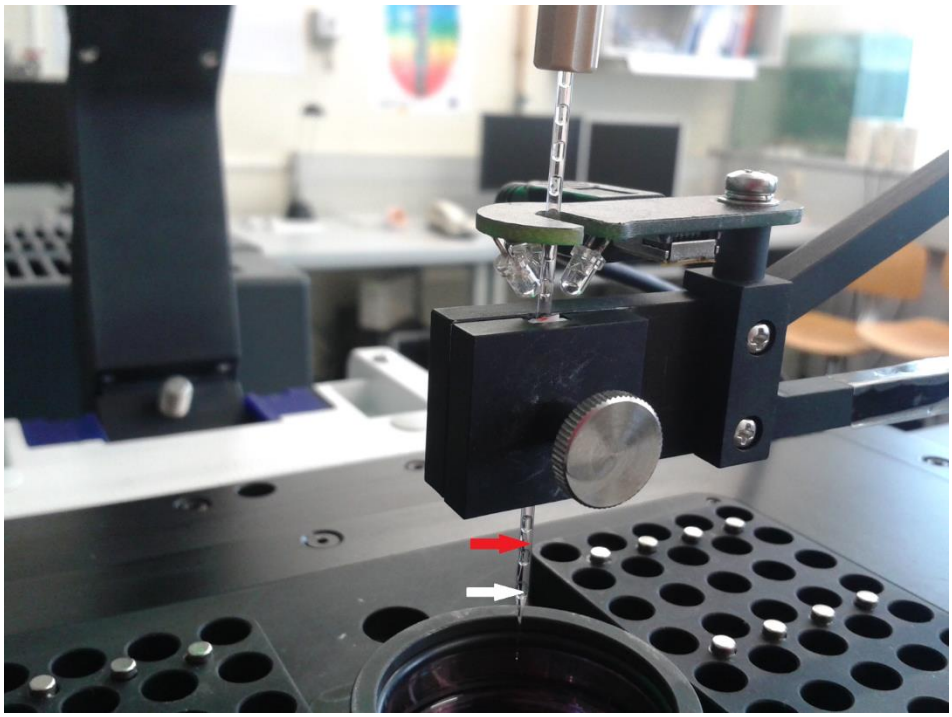

**Figure 1.** A micropipette with an I.D. of 70 μm containing single cells in the aqueous medium (labelled with red arrow in the picture) were separated from each other with oil layer (white arrow) to avoid the mixing of the individual cells inside the micropipette.

Using an optimized vacuum value for picking cells, isolation of 100 cells took ~ 42.5 min. Thus, I could not save time by separated cells from each other by a spacer oil layer as the isolation process slowed down due to the high viscosity of the oil.

In order to improve the speed of the sorting process, we maximized the speed of both the motorized microscope stage and the micromanipulator controlled by the CellSorter software. I optimized the velocity and acceleration of the hardware. I found that the optimal velocity and acceleration were 50 mm/s and 0.1 $m/s^2$ in case of the stage and 50 m/s and 2 $m/s^2$ in case of the manipulator.

I performed single cell sorting experiments with the accelerated instrument using NE-4C neuroectodermal mouse stem cells. I measured the speed of the method on two different hardware setups on three different sample holders (**Fig 2**):

1. 80 PCR tubes in the sample holder receiving single cells (at the Department of Eötvös University)
2. 2x96 Piko PCR plate (all together 192 wells) receiving single cells (at the Department of Eötvös University)

3. Standard 384-well tissue culture plate receiving single cells (at the Institute Technical Physics and Materials Science, Nanobiosensorics Laboratory).

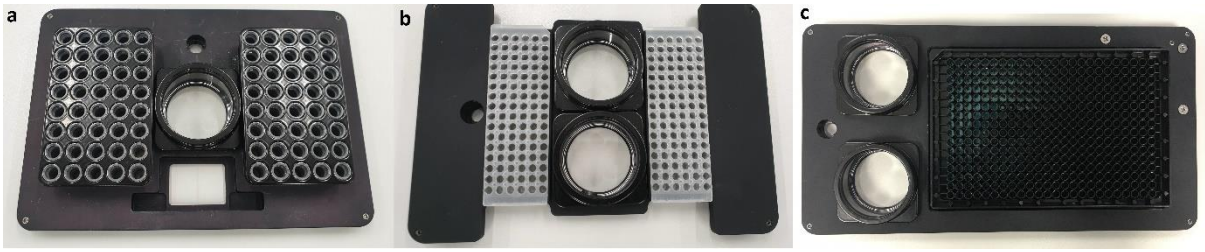


**Figure 2.** Sample holders used during sorting. **a)** sample holder with 80 PCR tubes **b)** PCR plate with 2 x 96 wells **c)** 384-well plate.

I could fill 80 PCR tubes with single cells in 13.5 min, within the target time interval of 15 min. Nevertheless, I had to decrease the acceleration of the microscope, when sorting cells from suspension[3] to avoid shaking the cells not attached to the surface of the Petri dish. The sorting speed in case of the three different sample holders and two different samples are shown in the *Table 1* below:

| **Type of sample holder** | **Sorting speed** | |
|---|---|---|
| | ***adherent cells*** | ***suspended cells*** |
| **80 PCR tubes** | 5.9 cell/min | 3.8 cell/min |
| **2x96-well Piko PCR plate** | 5.7 cell/min | 3.77 cell/min |
| **384-well standard tissue culture plate** | 3.4 cell/min | 3.27 cell/min |

**Table 1.** Single cell sorting speed with different type of sample holders and accelerated motorized microscope stage and micromanipulator.

I also quantitated the efficiency of single cell sorting when using the hardware with an increased velocity. When isolating NE-4C into 384-well plates, the single cell sorting efficiency was 74.5 ± 1.7%. 8.5 ± 0.3% of the picked-up cells were double cells and 17 ± 0.4% of the cells were not picked (n=129 single cells). The deposition efficiency was 87.5 ± 1.4%. Cell viability was

not investigated in the current study as we carried out an exhaustive viability experiment in our previous report[1,3].

## Development of a new piezoelectric micropipette

Liquid handling precision of commercially available micropipette-based methods is inherently limited by the long (~1 m) elastic plastic tube connecting the micropipette to the vacuum tank[1–3]. Although this limitation can be handled in research labs to achieve results in single cell RNA sequencing[4,5], circulating tumor cell (CTC) isolation[6], protein engineering[7] or single cell adhesion experiments[8,9], it hinders their routine application in medical diagnosis.

We developed a new piezoelectric micropipette[10] by CellSorter[11] for liquid handling in the nL range (**Fig 3**). It can be performed more accurate, more reliable manipulations than ever before at the level of individual cells. In contrast to the microliter precision instrument(s), we can routinely achieve subnanoliter precision, when pipetting volumes in the range of 0.5-10 nL. It eliminates plastic tubes, valves, syringes, and pressure tanks. For high-quality phase-contrast illumination of the sample, e.g., cells or tiny droplets, we constructed rings of LED-s arranged concentrically to the micropipette. It can be easily automated and integrated into various (bio)chemical workflows.

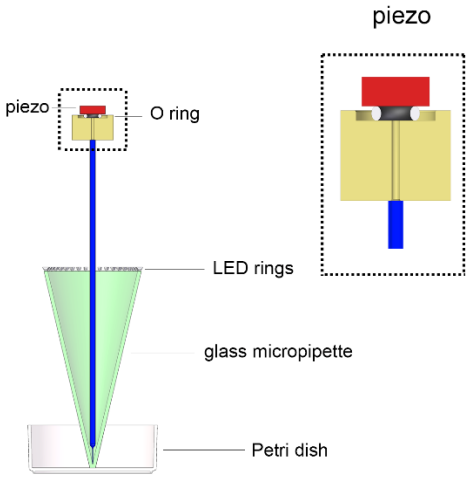


**Figure 3.** Schematic representation of the piezo micropipette. The piezo actuator at the top is pushed against an O-ring with sizes in the [1-6]x1 mm range. A glass micropipette is connected to the inner volume of the O-ring by a vertical channel. These are all filled with water. Phase contrast illumination is provided by a ring of LEDs arranged concentrically to the micropipette.

The glass micropipette is connected to a piezo actuator. Volume range of the pipette is set by the O-ring between the actuator and the glass micropipette; thus the same device can be applied in different volume ranges by exchanging the O-ring. Calibration of the micropipette proved that the device can be used in the [1–10] nl range.
We quantified the microscopic fluctuations of the fluid flow in the micropipette with particle tracking velocimetry of fluorescent microbeads. While the estimated flow rate of the peaks was 373±29 pl/s, the average volume fluctuation rate was 36±6 pl/s, resulting in a signal-to-noise ratio of 10.

I applied the piezoelectric micropipette for nL-scale droplet printing (**Fig 4**). I measured the volume of the printed droplets, and compared it to the full volume change of the pipette calculated from the displacement of the piezo actuator. I could control the volume of the printed droplets by the piezo voltage in the 10-60 nL range. Printed droplets were uniform with a standard deviation of a few nL. Volume of the droplets were lower than the calculated full volume of pipetting and it depended on the diameter of the micropipette due to the surface tension between water and oil.

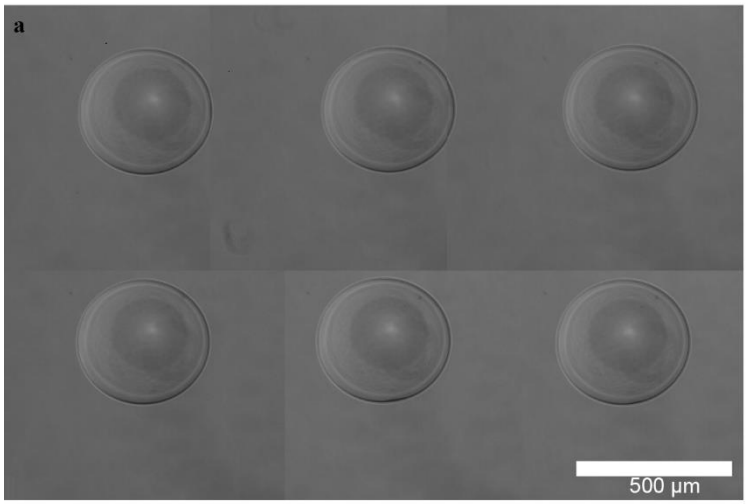


**Figure 4.** nL droplet printing. Water droplets printed with an I.D. 70 µm pipette (3.5x1.1 $mm^2$ O-ring) with +75 V under mineral oil.

It was also applied for single cell isolation from a suspension. It improved the efficiency of single-cell isolation from the previous ~75%[3] to above 90% without removing any neighbouring cell for 3T3, Jurkat, and HT-29 cells, respectively. We envision that this new technology will shortly become a standard tool for single-cell manipulations in medical diagnostics, e.g., circulating tumor cell isolation.

The new technology has been already implemented at the Karolinska Institutet in Stockholm and at the University of South Australia.

**Developing diffusion limited *in vitro* setup**

Usual *in vitro* cell cultures kept in macroscopic fluid volumes are not appropriate for investigating diffusion-limited processes due to the convection of the fluid. Previously, we applied a commercial 3D printer (Ultimaker) slightly modified to enable printing of multiwells into 35 mm Petri dishes[3]. We built miniature multi-well plates from polylactic acid (PLA) with a height of 0.5 or 1.0 mm into the Petri dish in order to keep suspended cells in a specified area of the dish (**Fig 5**). I used two structures[3] shown in **Fig 5**:

- two larger (5x5 $mm^2$) squares and 24 smaller (2x2 $mm^2$) squares for isolating single cells from a sparse culture (**Fig. 5a**)
- for the successive single cell isolation process from dense culture I used four 5x5 $mm^2$ squares (**Fig 5b**).

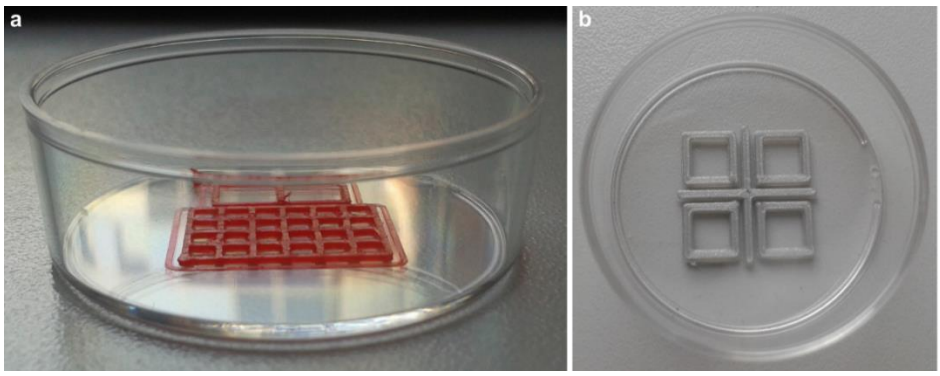


**Figure 5.** Photos of the miniature multiwell plates printed into 35 mm plastic Petri dishes with a resolution of 0.2 mm using a commercial 3D printer (Ultimaker).

My goal was to further minimize the convection[3] in the medium by applying 1x1x0.1 $mm^3$ microwells inside a Petri dish and develop a diffusion limited *in vitro* setup.

I created microwell arrays in 35 mm plastic Petri dishes with microthermoforming. First, silicon chip stamps used for microthermoforming were designed by the CellSorter Company in cooperation with the BioMEMS Group of the Institute of Technical Physics and Materials Science, Centre for Energy Research, Hungarian Academy of Sciences to achieve precise depth and smooth sidewalls in the forming wells. We produced silicon stamps with two different methods: KOH (potassium hydroxide) etching and DRIE (deep reactive-ion etching) fabricated with a height of 100 μm.

Then, I developed a custom hand press machine with a 0.1°C temperature precision. I explored both the temperature and the printing force dependence of the microthermoforming process. I achieved the most effective printing by heating up the Si chip stamp to 135°C and then pressing the heated chip into the Petri dish covered by silicon oil using weight until the chip cooled down to 115°C. Using Si wafers patterned by KOH method, the depth of the printed microwells was 30 µm (**Fig 6 a-b**), while using the DRIE Si wafers, the depth of the microwells was 45 µm (**Fig 6 c-d**) (instead of the planned 100 µm), measured in the scanning electron microscope (SEM) images.

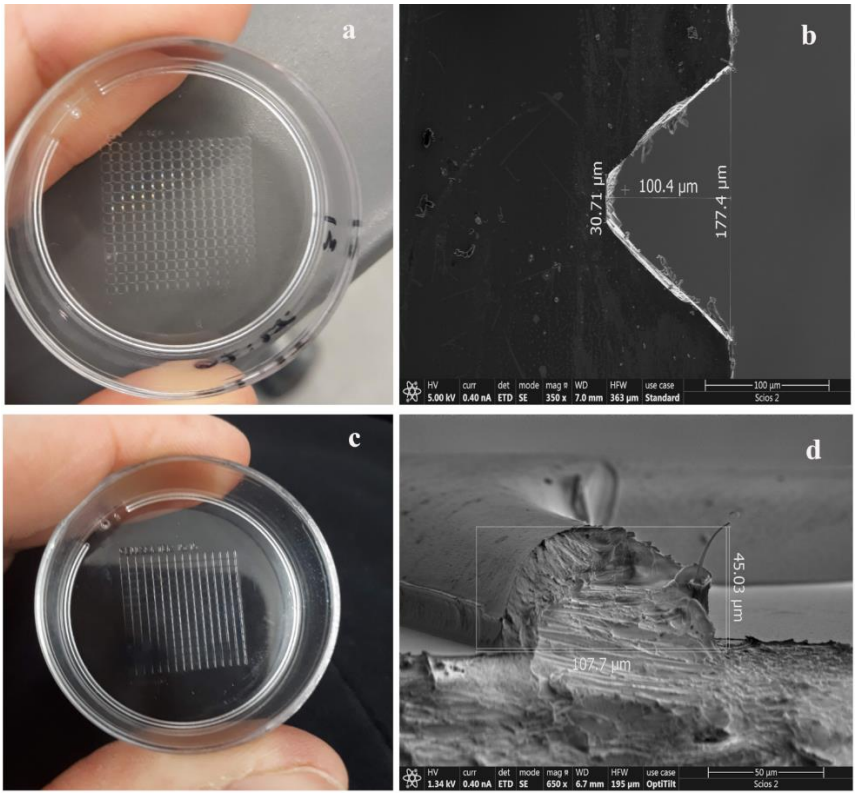


**Figure 6. a)** Petri dish with printed microwells by KOH method. **b)** Measuring the depth of printed microwells (can be seen in picture a) in the SEM images. **c)** Petri dish with printed microwells by DRIE method. **d)** Measuring the depth of printed microwells (can be seen in picture b) in the SEM images.

Cells were kept in a ~100 µm thin layer of the aqueous culture medium covered with mineral oil in order to minimize the fluid convection and evaporation of the medium. When sorting single cells, 3,000 Jurkat cells in 5 µl of culture medium were injected into a small area of the miniature multi-well plate under oil. I used the CellSorter piezoelectric micropipette to isolate single cells. I found that 33% of the selected cells were removed from their initial location due to a horizontal fluid flow during the sorting process. After the sorting process, the Petri dish with the microwells including single deposited cells was put into the $CO_2$ incubator to monitor their survival. I concluded that the shallow (depth of 30-45 µm), 1 mm wide square microwells

could not keep cells inside in the ~100 μm thick aqueous medium under oil. This prevented the efficient sorting and culturing of cells in these microwells. Thus, we decided to apply another method for this purpose: nanolitre aqueous droplet arrays kept under oil without microwells.

**Characterization of the dissolution of water microdroplets in oil**

To develop a nL droplet array for single cell cultures, I participated in a project to investigate the long-term behaviour of nL-scale water droplets in sparse water in oil (w/o) emulsions[12]. W/o emulsions consist of a continuous oil phase with dispersed water droplets. We generated emulsions in various oils using a simple rotating fluid-based method. Droplets were imaged by time-lapse microscopy and a modified contact angle measurement setup to investigate the evolution of their shape descriptors. Testing several oils, we observed that nL-sized water droplets dispersed in oil shrank and disappeared in a few hours. Application of surfactants did not have impact on the phenomenon. We determined analytically the product of the diffusion coefficient and the saturation density of water in oil. For my research, it is important to keep the nL-scale water droplets stable in the oil for several hours or days to realize the nL droplet array single cell cultures. For this, we have developed a technique to saturate mineral and silicone oils with water. (We saturated 20 ml of the oils by mixing them with deionized water with a magnetic stirrer (Biosan MSH 300) in a closed 50 ml upside down centrifuge tube at room temperature for more than 24 hours. The water to oil ratio was 50% in the tube.)

**Developing a pL scale luminescence-based detection method**

I could generate pL and nL-sized aqueous droplets with uniform size covered by mineral oil on a hydrophilic surface (Petri dish) using a glass micropipette.

I could readily use the piezoelectric[10] CellSorter instrument to automatically inject single 3T3 cells into the tiny (~ 0.5-1 nL) droplets using a micropipette with ID 30 μm (**Fig 7**). I applied a voltage of -2.5V to pick up single 3T3 cells and a voltage of +50V was needed to deposit single cells into an aqueous droplet under mineral oil layer. For successful droplet generation, the micropipette was positioned above the surface to 5 μm.

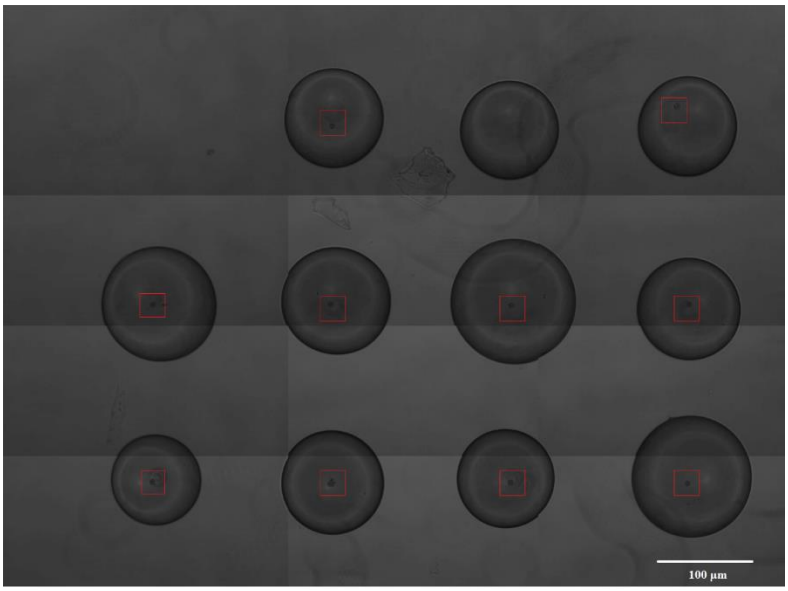


**Figure 7.** Phase contrast images of the deposited single 3T3 cells in the aqueous droplets covered by mineral oil layer. Red frames indicates single 3T3 cells in the droplets. 11 single 3T3 cells were selected for isolation; however, deposition of #10 cell was unsuccessful. Cells were labelled with DiI. Scale bar: 100 µm.

I could also deposit nL droplets containing a dense culture of U 937 cells (**Fig 8**). Droplets were generated using the valve system[2] of the CellSorter instrument with a micropipette of ID 70 µm. First, dense culture of cells were sucked into the micropipette. A vacuum of -100 Pa was generated in syringe 1 using syringe pump (Valve1). Hydrostatic injection pressure in syringe 2 was 9,800 Pa (Valve 2). I could controll the drop volume with the duration of valves opening: Valve 1 was opened for 200 ms, Valve 2 for 1000 ms and delay was 1000 ms. Micropipette approached the surface to 50 µm when generating the droplets. Height of the deposited droplets were ~20 µm.

With this method, using two different cell types I can investigate cell-to-cell communication in a nL-scale volume.

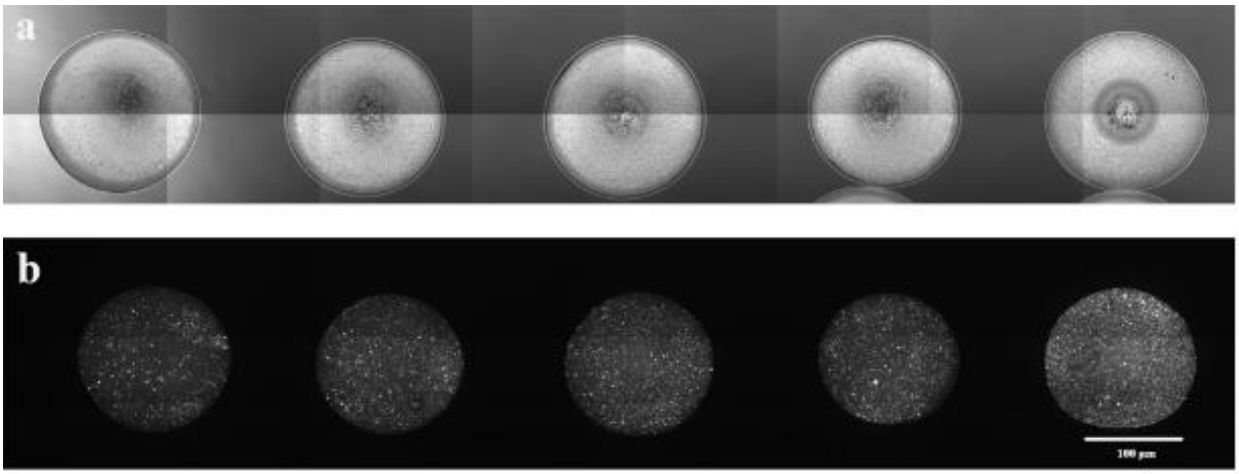


**Figure 8.** nL aqueous droplets containing a dense culture of U 937 cells in a Petri dish. Phase contrast **(a)** and fluorescent **(b)** images of 5 deposited water droplets containing a dense culture of suspension U 937 cells. Cells were labelled with DiI. Scale bar: 100 μm.

I performed introductory experiments to determine the concentration of soluble components (ATP) *in situ* with luminescent reagents. I generated pL water droplets in Petri dishes using a micropipette with ID 70 μm (**Fig 9**).

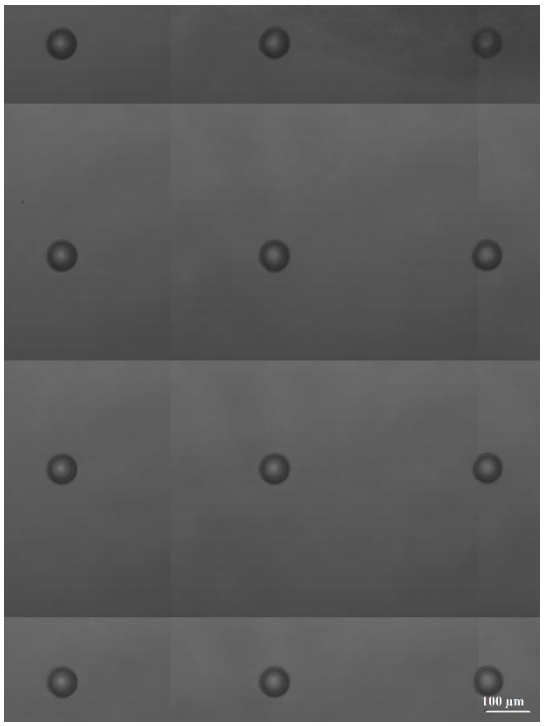


**Figure 9.** Picoliter droplet printing. Water droplets printed with an I.D. 70-μm pipette. Scale bar: 100 μm.

Then I applied a small diameter micropipette (ID 1 μm) filled with 0.5 μm fluorescent microbeads to inject the beads into the pL-sized droplets. Fluorescent beads were used to simulate the injection of the luminescent ATP indicator into the pL droplet to test the success

of the process. My aim was to change water and the fluorescent beads to ATP and the luminescent ATP indicator, respectively. I wanted to continue this experiment in the 3rd year of my project and measure the eATP concentration in the nL scale microenvironment of live cells using the piezoelectric micropipette.

**Studying the adhesion force of individual cells**

Cell adhesion is a fundamental phenomenon in biology. Numerous studies focused on its function in biological and medical processes. The computer-controlled micropipette which can isolate individual cells, it can be also used to study cell-to-cell[13] or single cell-to-specific macromolecule[8,9] interactions. Several techniques have been developed or are under development to quantify cell adhesion. All of them have their pros and cons, which has to be carefully considered before the experiments and interpretation of the recorded data.

I thought that, writing a comprehensive review article to provide a practical guide for scientists to choose the appropriate technique for measuring cell adhesion *in vitro* would be important[14]. So I divided into two categories the techniques that can be used to determine the strength of adhesion: population methods and single-cell approaches. Most important parameters to be considered are the i) number of cells to be measured, ii) range of the adhesion force, iii) duration of the experiment. I identified the major advantages and disadvantages of each method.

**Single-cell adhesion strength and contact density drops in the M phase of cancer cells**

Cell adhesion[15] is a fundamental and complex biological process of a cell anchoring to another cell or to the extracellular matrix (ECM). This process is mediated by cell surface receptor molecules[16]. Cell adhesion is known to be closely related to the actin cytoskeleton, the organization of which is crucial in determining the structural and mechanical properties of living cells. Dynamically controlled cell adhesion plays a cardinal role both on the level of individual cells in intracellular signaling, migration, proliferation, differentiation, and gene expression and on the level of multicellular organisms in cell–cell communication, the developing embryo[16], the immune system[17], and the metastasis of tumors[18–20].

For most cells, cell cycle progression is anchorage-dependent[21], requiring cell–ECM interactions via integrin transmembrane receptors and the formation of actin-associated adhesion complexes[22]. G1 and G2 phases are characterized by cell growth which includes an increase in the area of contact between the cell and its substrate. Early observations on flat

surfaces have shown that directly before mitosis (the M phase of the cell cycle), focal adhesion complexes and actin stress fibers are rapidly disassembled. This results in a drastic reduction of traction forces[23] and previously spread out cells round up due to a radical reorganization of the cytoskeleton[24]. This cell rounding is required for accurate spindle formation and chromosome capture and the integrin-mediated adhesion is required for determining the orientation of cell division[25].

I investigated and compared cell adhesion strengths throughout the cell cycle at the single-cell level[26] using two complementary methods: computer-controlled micropipette (CCMP)[8] and a high spatial resolution RWG optical biosensor (commonly recognized as Epic Cardio)[27] to determine how the strength of adhesion of cells to the surface varies during the progression of the cell cycle. I used a synthetic polymer RGD-functionalized poly(L-lysine)-graft-poly(ethylene glycol) (PLL- g-PEG-RGD)-coated surface. As a cell cycle reporter, I used the Fucci fluorescent construct in HeLa cells[28]. Fucci expresses two different fluorescent reporter proteins in a time-varying quantity during the cell cycle. I categorized cells into four groups based on their fluorescent intensity: red cells (G1 phase), yellow cells (beginning of the S phase), green cells (S/G2/M phase), and colorless cells (transition from M to G1 phase).

Using CCMP, I revealed that colorless cells needed a much lower hydrodynamic lifting force to be picked up from the surface than the colored cells did. No significant difference between the adhesion strength of red, yellow and green cells. Optical biosensor measurements confirmed the weaker adhesion of colorless cells. Comparison of colored cells revealed no significant difference in the sensor signal. I found that, the results of the two different techniques are in line (**Fig 10**). The adhesion strength of single cells is constant in all phases of the cell cycle except the M phase with a significantly lower adhesion.

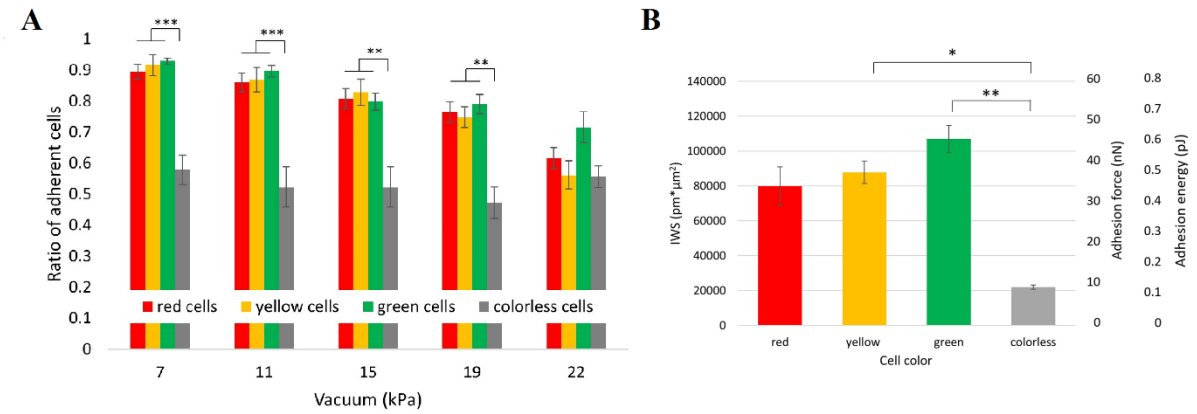


**Figure 10. (A)** Ratio of adherent HeLa Fucci cells on PLL-g-PEG-RGD surface at different vacuum values, as measured by the computer-controlled micropipette. * indicates significant difference between the ratio of different

cell phases. **(B)** Correlation between cell color and integral of wavelength shift (IWS), adhesion energy, and adhesion strength. A significant difference was found between colorless cells with respect to green and yellow cells.

My results are directly comparable with other works in the literature on single-cell force spectroscopy[29,30], with the prominent advantage over them, being a non-invasive, label-free, and real-time method. Moreover, the developed methodologies are ready to be employed in more complex lab on a chip system for industrial applications, to test the effect of novel drug candidates on cancer cells during their cell cycle progression. I believe that cell adhesion can be a new tumour therapeutic target because its strength is significantly reduced at the end of the M phase. Since this is a short period of the cell cycle, the effect of a drug can be specific to the rapidly dividing tumor cells. I believe the experimental techniques used in this study and the results provided by them to be of aid to develop novel integrin targeting drugs.

## Nanonewton scale force measurements on biotinylated microbeads with a robotic micropipette

Computer-controlled micropipette[8,9,13,14] can quantify the surface adhesion of live cells[8] or functionalized microparticles[31] with relatively high throughput (hundreds of cells/beads in 30 min)[32]. New computational fluid dynamics (CFD) simulations were constructed to calculate the hydrodynamic forces acting on biotinylated 10 μm beads on avidin coated surfaces to determine the unbinding force of beads[33]. Using the micropipette setup, I measured the aspiration pressure needed to remove the surface attached microbeads by targeting them manually on the microscope. My goal was to experimentally determine the effect of the targeting offset on the hydrodynamic lifting force. The bead was positioned into the center (axis) of the micropipette or to a 5, 10, 15 or 20 μm horizontal offset from that. To achieve proper robotic bead targeting, I used the adaptive targeting[3] algorithm of the CellSorter software. Measuring the vacuum needed to pick up the beads and converting the experimental vacuum to a hydrodynamic lifting force on the basis of simulations, I found an unbinding force of 12±2 nN, when targeting the beads manually; robotic targeting resulted in 9±4 nN. According to the simulations, the higher offset resulted in a higher lifting force acting on the bead. Considering this effect, we could readily correct the impact of the targeting offset to renormalize the experimental data. Horizontal force and torque also appeared in simulations in case of a targeting offset.

Surprisingly, simulations showed that the lifting force acting on the bead reaches a maximum at a flow rate of ~ 5 μl/s if the targeting offset is <5 μm. Further increasing the flow rate

decreases the lifting force. I attribute this effect to the spherical geometry of the bead. I predict that higher flow rates cannot increase the hydrodynamic lifting force acting on the precisely targeted microbead, setting a fundamental force limit (16 nN in our setup) for manipulating microbeads with a micropipette perpendicular to the supporting surface. In order to extend the force range, I propose the offset targeting of microbeads.

Today, the gold standard of nanonewton scale force measurements is the AFM[34,35]. A modified AFM, the fluidic force microscope (FluidFM) provides higher throughput by reversibly fixing the targeted bead on a hollow cantilever using vacuum, in contrast to irreversible chemical attachment on a traditional AFM cantilever[31,36]. Major advantage of our method - originally developed for picking single live cells - is its non-contact nature. The micropipette does not touch the microbead when probing the adhesion force allowing even higher throughput than FluidFM in a robotic setup. This non-contact nature minimizes the possible contamination of both the micropipette and the targeted bead especially useful for probing a large number of microbeads.

I expect that the micropipette-microbead based method introduced here will be applied to measure the detachment force of many more molecular interactions and will be widely employed to characterize the binding forces between surfaces. It is suitable for comparative studies, e.g., to investigate the effect of a specific drug or protein/ligand modifications on surface-to-surface interactions in a simple, automated, and high throughput manner.

## References


1. Környei, Z. *et al.* Cell sorting in a Petri dish controlled by computer vision. *Sci. Rep.* **3**, 1088 (2013).

2. Salánki, R. *et al.* Automated single cell sorting and deposition in submicroliter drops. *Appl. Phyisics Lett.* **105**, 083703 (2014).

3. Ungai-Salánki, R. *et al.* Automated single cell isolation from suspension with computer vision. *Sci. Rep.* **6**, 20375 (2016).

4. Kozlov, A. *et al.* A Screening of UNF Targets Identifies Rnb , a Novel Regulator of Drosophila Circadian Rhythms . *J. Neurosci.* **37**, 6673–6685 (2017).

5. Ngara, M. *et al.* Exploring parasite heterogeneity using single-cell RNA-seq reveals a

gene signature among sexual stage Plasmodium falciparum parasites. *Exp. Cell Res.* **371**, 130–138 (2018).

6. Winter, M. *et al.* Isolation of Circulating Fetal Trophoblasts Using Inertial Microfluidics for Noninvasive Prenatal Testing. *Adv. Mater. Technol.* **3**, 1800066 (1–10) (2018).

7. Piatkevich, K. D. *et al.* A robotic multidimensional directed evolution approach applied to fluorescent voltage reporters. *Nat Chem Biol.* **14**, (2018).

8. Salánki, R. *et al.* Single Cell Adhesion Assay Using Computer Controlled Micropipette. *PLoS One* **9**, e111450 (2014).

9. Sándor, N. *et al.* CD11c / CD18 Dominates Adhesion of Human Monocytes , Macrophages and Dendritic Cells over CD11b / CD18. *PLoS One* **11**, e0163120 (2016).

10. Francz, B., Ungai-Salánki, R., Sautner, É., Horvath, R. & Szabó, B. Subnanoliter precision piezo pipette for single-cell isolation and droplet printing. *Microfluid. Nanofluidics* **24**, 1–10 (2020).

11. CellSorter Kft. (2019) Piezoelectric micropipette PCT patent application HU 2019/000002. Piezoelectric micropipette.

12. Gerecsei, T. *et al.* Characterization of the Dissolution of Water Microdroplets in Oil. *Colloids and Interfaces* **6**, (2022).

13. Jani, P. K. *et al.* Complement MASP-1 enhances adhesion between endothelial cells and neutrophils by up-regulating E-selectin expression. *Mol. Immunol.* **75**, 38–47 (2016).

14. Ungai-Salánki, R. *et al.* A practical review on the measurement tools for cellular adhesion force. *Adv. Colloid Interface Sci.* **269**, 309–333 (2019).

15. Bachir, A. I., Horwitz, A. R., Nelson, W. J. & Bianchini, J. M. Actin-based adhesion modules mediate cell interactions with the extracellular matrix and neighboring cells. *Cold Spring Harb. Perspect. Biol.* **9**, (2017).

16. Bruce Alberts, Alexander Johnson Julian Lewis, Martin Raff,Keith Roberts, P. W. *Molecular biology of the cell*. (Garland Science., 2007).

17. Ley, K., Laudanna, C., Cybulsky, M. I. & Nourshargh, S. Getting to the site of inflammation: the leukocyte adhesion cascade updated. *Nat. Rev. Immunol.* **7**, 678–689 (2007).

18. Albelda, S. M. Role of integrins and other cell adhesion molecules in tumor progression and metastasis . *J. Tech. Methods Pathol.* **68**, 4–17 (1993).

19. Rao, C. C. G. *et al.* Expression of epithelial cell adhesion molecule in carcinoma cells present in blood and primary and metastatic tumors. *Int. J. Oncol.* **27**, 49–57 (2005).

20. Kobayashi, H., Boelte, K. C. & Lin, P. C. Endothelial cell adhesion molecules and cancer progression. *Curr. Med. Chem.* **14**, 377–386 (2007).

21. Schulze, A. *et al.* Anchorage-dependent transcription of the cyclin A gene. *Mol. Cell. Biol.* **16**, 4632–4638 (1996).

22. Park, J. H., Arakawa-Takeuchi, S., Jinno, S. & Okayama, H. Rho-associated kinase connects a cell cycle-controlling anchorage signal to the mammalian target of rapamycin pathway. *J. Biol. Chem.* **286**, 23132–23141 (2011).

23. Lesman, A., Notbohm, J., Tirrell, D. A. & Ravichandran, G. Contractile forces regulate cell division in three-dimensional environments. *J. Cell Biol.* **205**, 155–162 (2014).

24. Dao, V. T., Dupuy, A. G., Gavet, O., Caron, E. & de Gunzburg, J. Dynamic changes in Rap1 activity are required for cell retraction and spreading during mitosis. *J. Cell Sci.* **122**, 2996–3004 (2009).

25. Mathew, S. S. *et al.* Integrins promote cytokinesis through the RSK signaling axis. *J. Cell Sci.* **127**, 534–545 (2014).

26. Ungai-Salánki, R. *et al.* Single-cell adhesion strength and contact density drops in the M phase of cancer cells. *Sci. Rep.* **11**, 1–13 (2021).

27. Sztilkovics, M. *et al.* Single-cell adhesion force kinetics of cell populations from combined label-free optical biosensor and robotic fluidic force microscopy. *Sci. Rep.* **10**, (2020).

28. Sakaue-Sawano, A. *et al.* Visualizing Spatiotemporal Dynamics of Multicellular Cell-Cycle Progression. *Cell* **132**, 487–498 (2008).

29. Panagiotakopoulou, M. *et al.* Cell cycle-dependent force transmission in cancer cells.

*Mol. Biol. Cell* **29**, 2528–2539 (2018).

30. Vianay, B. *et al.* Variation in traction forces during cell cycle progression. *Biol. Cell* **110**, 91–96 (2018).

31. Gerecsei, T. *et al.* Adhesion force measurements on functionalized microbeads: An in-depth comparison of computer controlled micropipette and fluidic force microscopy. *J. Colloid Interface Sci.* **555**, 245–253 (2019).

32. Gerecsei, T. *et al.* Prospects of fluidic force microscopy and related biosensors for medical applications. *Nanobioanalytical Approaches to Med. Diagnostics* 1–28 (2022). doi:10.1016/B978-0-323-85147-3.00014-1

33. Ungai-Salánki, R. *et al.* Nanonewton scale adhesion force measurements on biotinylated microbeads with a robotic micropipette. *J. Colloid Interface Sci.* **602**, 291–299 (2021).

34. Yu-Shiu Lo, Ying-Jie Zhu, and Thomas P. Beebe, J. Loading-Rate Dependence of Individual Ligand-Receptor Bond-Rupture Forces Studied by Atomic Force Microscopy. *Langmuiry* **17**, 3741–3748 (2001).

35. Binnig, G. & Quate, C. F. Atomic Force Microscope. *Phys. Rev. Lett.* **56**, 930–933 (1986).

36. Dörig, P. *et al.* Exchangeable colloidal AFM probes for the quantification of irreversible and long-term interactions. *Biophys. J.* **105**, 463–472 (2013).